the FEBS Journal

Regional and segmental flexibility of antibodies in interaction with antigens of different size

Masayuki Oda[1], Susumu Uchiyama[2], Carol V. Robinson[3], Kiichi Fukui[2], Yuji Kobayashi[4] and Takachika Azuma[5]

1 Graduate School of Agriculture, Kyoto Prefectural University, Japan
2 Graduate School of Engineering, Osaka University, Japan
3 Department of Chemistry, University of Cambridge, UK
4 Graduate School of Pharmaceutical Sciences, Osaka University, Japan
5 Research Institute for Biological Sciences (RIBS), Tokyo University of Science, Chiba, Japan

Keywords
antigen–antibody interaction; analytical ultracentrifugation; electrospray ionization time-of-flight mass spectrometry; protein flexibility; surface plasmon resonance

Correspondence
T. Azuma, Research Institute for Biological Sciences (RIBS), Tokyo University of Science, 2669, Yamazaki, Noda, Chiba 278-0022, Japan
Fax: +81 4 7121 4089
Tel: +81 4 7121 4082
E-mail: tazuma@rs.noda.tus.ac.jp

(Received 29 November 2005, accepted 6 February 2006)

doi:10.1111/j.1742-4658.2006.05168.x

The interaction of antibodies (Abs) with protein antigens (Ags) of different size, such as hen egg white lysozyme, ovalbumin, and bovine serum albumin, was examined using analytical ultracentrifugation, electrospray ionization time-of-flight mass spectrometry, and surface plasmon resonance in order to estimate regional and segmental Ab flexibility. When both Abs and Ags were free in solution, sedimentation equilibrium and surface plasmon resonance analyses showed the formation of an Ag_2Ab_1 complexes regardless of Ag size, suggesting that the Fab arms were able to move to avoid interference between Ags bound to Ab combining sites. The Ag_2Ab_1 complex, as well as the Ag_1Ab_1 complex, was observed by MS. However, when Abs were immobilized on the surface of a sensor chip through the Fc region, the stoichiometry of the Ag–Ab complex was dependent on the Ag size; Ag_2Ab_1 forming with hen egg white lysozyme and Ag_1Ab_1 with ovalbumin and bovine serum albumin. These results indicated that immobilization of the Fc region reduces the dynamic range of the Fab arms and results in interference from the first Ag bound to either combining site, which in turn prevents the binding of the second Ag to the other combining site. Our results allow us to propose that the Fab arms of B-cell receptors whose Fc regions are immobilized on cell surface have a reduced dynamic range.

Introduction

Antibodies (Abs) exist in body fluid or on B cells as antigen (Ag) receptors (BCRs). They are capable of binding to a vast array of Ags of different shape and size such as soluble proteins in solution or membrane proteins on micro-organisms. It is well known that the cooperative binding of Abs to multivalent Ags using multiple combining sites, two for an IgG and 10 for an IgM pentamer, enhances the apparent binding affinity, which is termed avidity. The avidity is increased when two Fab arms of an Ab simultaneously interact with the epitopes of an Ag. Such multivalent interaction between Ag and Ab would depend on the distribution of epitopes and the flexibility of the Fab arms. The IgG molecule consists of two Fab arms and one Fc region, the latter being responsible for the immunological effector function. It has long been debated whether the effector function of an Ab is induced by Ag binding [1].

Structural analyses by X-ray crystallography have provided precise information on three-dimensional structures of monoclonal antibodies (mAbs) at atomic

Abbreviations
Ab, antibody; Ag, antigen; AUC, analytical ultracentrifugation; BCR, B-cell antigen receptor; BSA, bovine serum albumin; cryo-ET, cryo-electron tomography; HEL, hen egg white lysozyme; K_a, equilibrium association constant; k_{off}, dissociation rate constant; k_{on}, association rate constant; mAb, monoclonal antibody; OVA, ovalbumin; RAMFc, rabbit anti-(mouse Fc) IgG; RU, response unit; TOF, time-of-flight.

 © 2006 The Authors Journal compilation © 2006 FEBS

resolution. The molecular structure of two intact mAbs, IgG1 and IgG2a, were determined [2,3], and showed that IgG1 has an angle of 115° between two Fab arms so that it exhibits a 'distorted Y shape', whereas IgG2a has an angle of 172° and therefore exhibits a 'distorted T shape'. However, immunoelectron microscopy showed that the Fab–Fab angle of human IgG1 is 117 ± 43° [4], and cryo-electron tomography (cryo-ET) studies recently showed that the positions of the Fab arms relative to the Fc region of a monoclonal IgG2a differ greatly from one molecule to another, and the Fab–Fab angle ranges between 88 and 141° [5,6]. These findings are quite different to those obtained from the crystal structure of the same subclass [2], and demonstrate the difficulty in interpreting overall protein structures of flexible proteins using X-ray crystallography alone, because the crystal structure obtained is mainly one of many possible 'snapshots' due to the wide spectrum of attainable conformers present in solution.

The number of Ags capable of simultaneously binding to an Ab, a property referred to as stoichiometry, varies according to the Ag size and dynamic range of the two Fab arms, and estimating the stoichiometry has proven useful for understanding protein flexibility and function. For this purpose, wide use has been made of sedimentation equilibrium analysis, a powerful application of analytical ultracentrifugation (AUC) [7]. Recently, a combination of electrospray ionization (ESI) and time-of-flight (TOF) MS using a gentle desolvation technique under controlled pressure has been applied to study noncovalently associated protein complexes, such as chaperon oligomers [8], protein–micelle complex [9], and even whole ribosome [10]. Binding stoichiometry between V Ag and its Ab was also investigated using MS [11]. The extremely high resolution of MS has enabled us to determine the exact stoichiometry of the complex in the gas phase, which reflects their interaction state in solution. Furthermore, we recently showed that surface plasmon resonance (SPR) provided a convenient means of determining the binding stoichiometry, together with its general application in determination of binding kinetics [12–14]. In these experiments, mouse mAbs were captured through their Fc regions by a rabbit anti-(mouse Fc) IgG (RAMFc) that was chemically attached to a sensor chip surface. This has an advantage over immobilizing the mAbs directly, because the two Fab arms would have freedom of movement.

In this study, we prepared mAbs against hen egg white lysozyme (HEL, 14 kDa), ovalbumin (OVA, 45 kDa), and bovine serum albumin (BSA, 67 kDa), and analyzed the binding stoichiometry and kinetics in Ag–mAb interactions using AUC, MS, and SPR analyses. AUC and MS provide information about interactions between Ag and mAb when both are free in solution, whereas SPR is useful when either component, Ag or mAb, is immobilized on the surface of a sensor chip. We considered that the immobilized Ags would act as a model of multivalent Ags on a microorganism membrane and the immobilized mAbs would act as a model of BCRs. By comparing the results obtained with these different methods, we are able to analyze the effects of Fc immobilization on the flexibility of Fab arms considering our recent finding that the binding of Ag to Ag-combining sites induced fine conformational changes in the constant domain, which were expected to have a critical effect on intracellular signaling via BCRs [15,16]. From this point of view, we were interested in determining whether the restriction of regional movement by anti-Fc IgG affects the segmental flexibility of the two Fab arms within which the Ag-combining sites are located.

Results

Interaction between free Ags and free mAbs in solution observed by AUC

In order to analyze the binding stoichiometry between OVA or BSA and monoclonal anti-OVA mAb (O1-1) or monoclonal anti-BSA mAb (KM10), sedimentation equilibrium analysis was carried out. At first, the molecular masses of Ag and mAb in solution were estimated separately. For each Ag and mAb solution, the apparent molecular mass at different concentration agreed with the value calculated from the amino acid composition and had no protein concentration dependency (data not shown), indicating that each protein was a monomer and monodisperses under the experimental conditions used.

Mixtures of Ag and mAb were then centrifuged and the resulting equilibrium concentration gradients of mixtures of Ag and mAb were subjected to nonlinear least-squares fitting using a 1 : 1 or 2 : 1 (Ag/mAb) interaction model. In the case of an interaction between O1-1 and OVA (Fig. 1A), residuals for the 2 : 1 model were distributed randomly, whereas those for the 1 : 1 model were rather unevenly distributed at all molar ratios used. Consistent with these results, χ^2 values for fitting with the 2 : 1 model were smaller than those for the 1 : 1 model. These results indicate that the 2 : 1 model was a better fit than the 1 : 1 model. Furthermore, at an Ag-to-mAb molar ratio of 3 : 1, the 2 : 1 model gave a better fit than the 1 : 1 model (Fig. 1A, right), showing that the 2 : 1 complex is dominant in the presence of excess Ag.

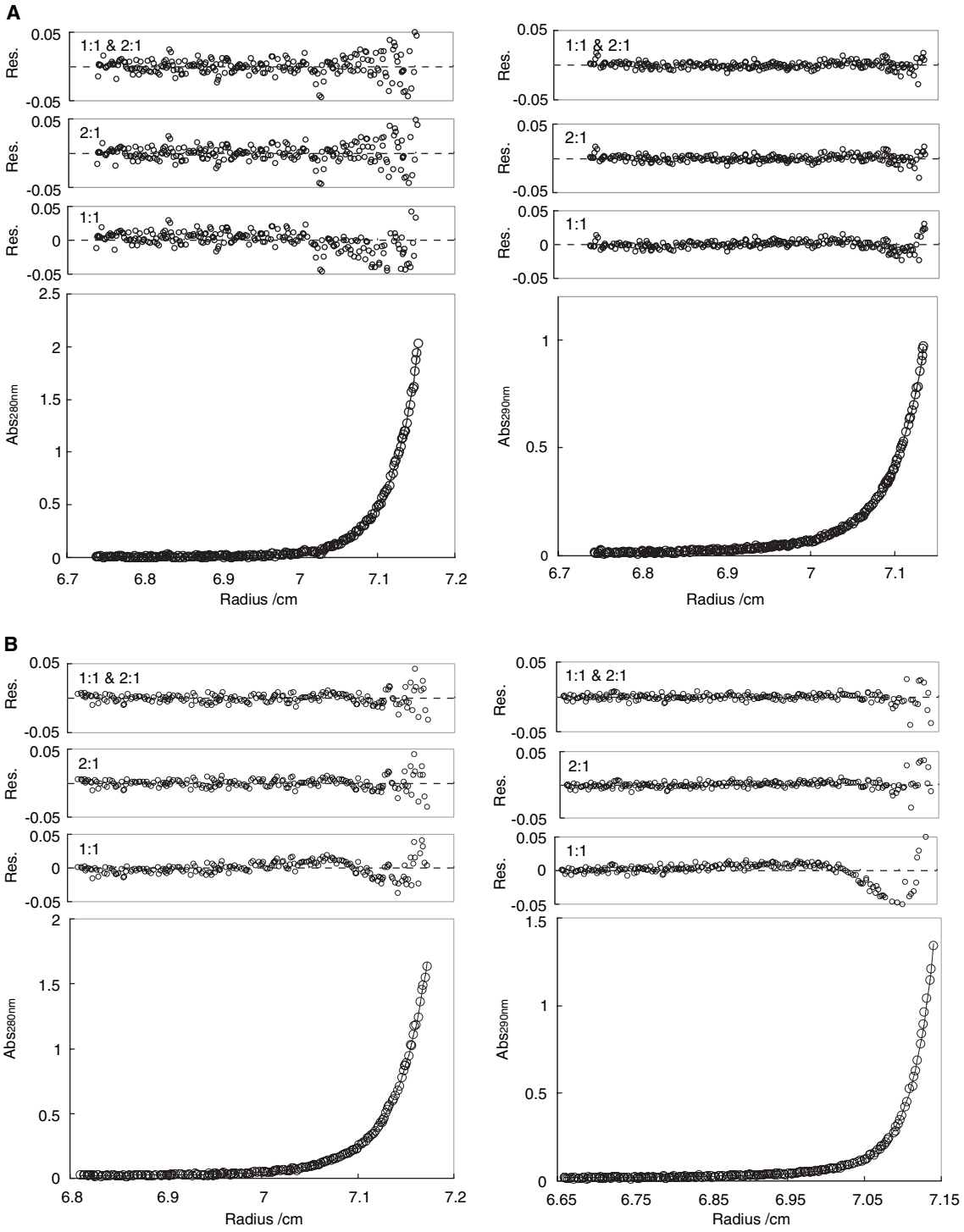


Fig. 1. Sedimentation equilibrium data obtained at 280 or 290 nm, best fit results, and the corresponding residuals using three different models (1 : 1, 2 : 1, and 1 : 1 and 2 : 1 coexisting models) for the interactions between OVA or BSA and anti-OVA mAb or anti-BSA mAb. (A) A solution of OVA and O1-1 anti-OVA mAb was mixed in an equimolar ratio (left) and in a 3 : 1 molar ratio (right). (B) A solution of BSA and KM10 anti-BSA mAb was mixed in an equimolar ratio (left) and a 6 : 1 molar ratio (right). The line through the data represents the best fit for the 2 : 1 association model.

Similarly, all sedimentation profiles of a mixed solution of BSA and KM10 under different molar ratios were better fits with the 2 : 1 model than with the 1 : 1 model (Fig. 1B). In addition to the equal distributions of residuals, χ^2 values for the 2 : 1 model were smaller than those for the 1 : 1 model, further supporting 2 : 1 binding stoichiometry between BSA and KM10. Fits of sedimentation data using coexisting 1 : 1 and 2 : 1 models for different Ag concentrations in excess of those of mAbs provided only slightly improved residual patterns compared with those of the 2 : 1 model (Fig. 1B). Our results indicate that the Ag_2Ab_1 complex is dominant, particularly when there is a higher Ag to mAb ratio. The equilibrium association constants (K_a) obtained from the fitting were 3.4×10^5 M^{-1} for O1-1 and 1.1×10^8 M^{-1} for KM10.

Interaction between free Ags and free mAbs in solution observed by MS

Figure 2A shows the mass spectrum of YOVA anti-OVA mAb. Well-resolved peaks with different charge

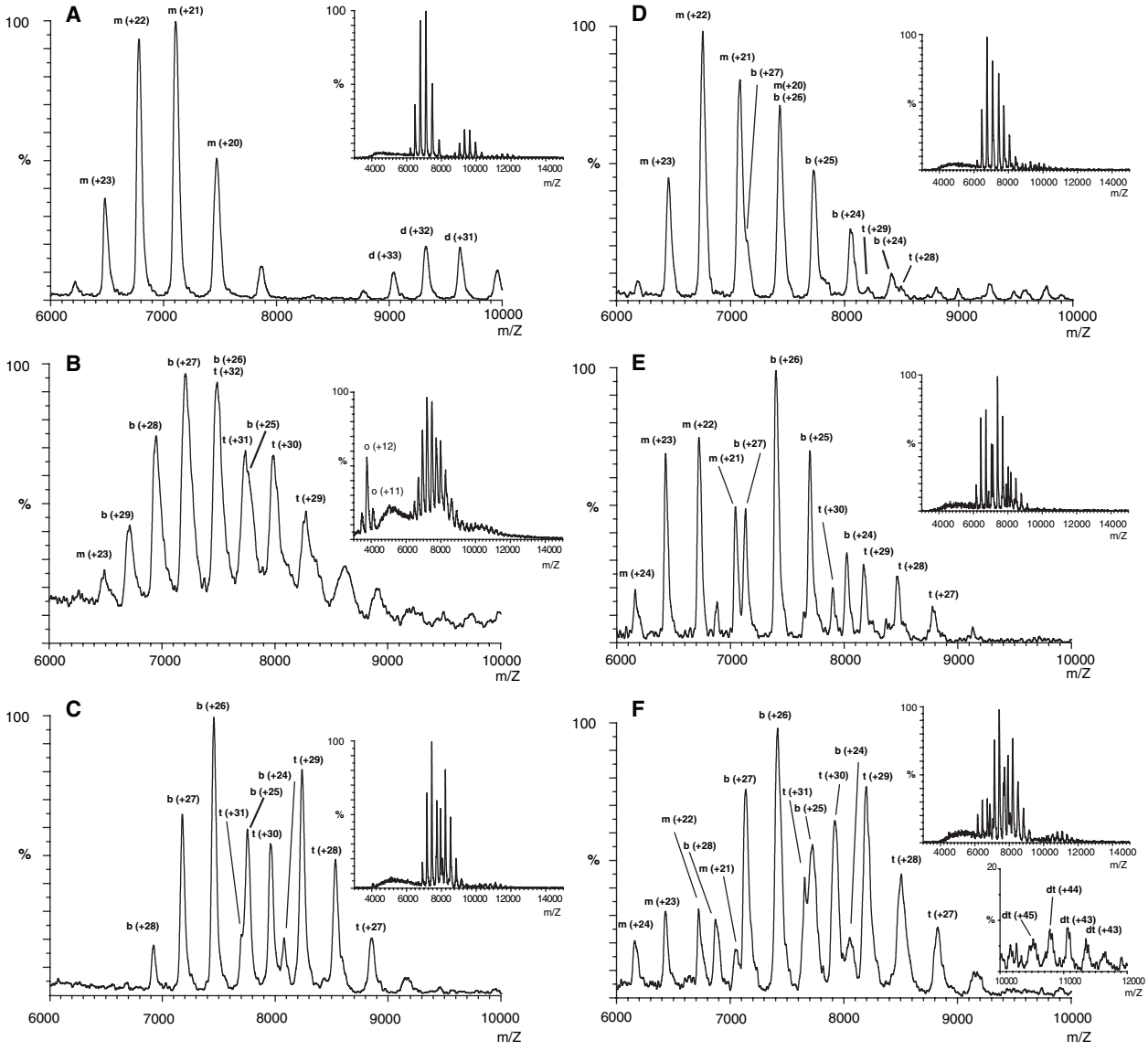


Fig. 2. MS of YOVA anti-OVA and mixed solutions of OVA and its mAbs, YOVA and O1-1. (A–C) MS of YOVA (A), of a mixed solution of OVA and YOVA for an equimolar ratio (B), and for a 3 : 1 molar ratio (C). (D–F) MS of a mixed solution of OVA and O1-1 for an equimolar ratio (D), a 3 : 1 molar ratio (E) and a 6 : 1 molar ratio (F). Inserts show overall MS with m/*z*-value of 3000–15 000. The peaks labeled m and d represent monomer and dimer form of mAbs, respectively, and b, t, and dt represent Ag_1Ab_1, Ag_2Ab_1, and Ag_4Ab_2 complexes, respectively. The charge states are given in parentheses. The peaks labeled o represent unbound OVA.

Table 1. Calculated and measured masses for OVA, monoclonal anti-OVA mAbs, and their complexes.

Protein complex	Measured mass (Da)	Calculated mass (Da)
OVA	44 633 ± 3	
YOVA	149 233 ± 45	unknown
OVA–YOVA	194 652 ± 64	193,866
OVA_2–YOVA	239 714 ± 41	238,499
O1-1	148 768 ± 33	unknown
OVA–O1-1	194 446 ± 38	193,401
OVA_2–O1-1	237 997 ± 56	238,034

states were observed. These patterns are in good agreement with that of mAb 7.3, a mAb against V Ag, observed previously [11]. The assignment of series of charge states enabled the calculation of the mass of mAbs, as reported in Table 1. A second series of charge states for mAb dimers were also observed at lower intensities.

The mass spectra recorded for a mixed solution of mAb, YOVA, and its Ag, OVA, are shown in Fig. 2B,C. At an equimolar ratio of OVA and YOVA, additional series of peaks are observed in addition to peaks of charge states from unbound YOVA with weak intensities and unbound OVA. Assignment of their *m/z*-values gave two series of peaks with average charges of +26 and +29 and molecular masses in close agreement with those for a complex formed between one molecule of OVA and one molecule of YOVA (Ag_1Ab_1 complex) and those for a complex formed between two molecules of OVA and one molecule of YOVA (Ag_2Ab_1 complex). Increasing the OVA concentration in excess of the YOVA concentration resulted in the disappearance of unbound YOVA peaks, and peaks for the Ag_2Ab_1 complex became prominent at a 3 : 1 excess of OVA to YOVA (Fig. 2C). Mass spectrum at a 6 : 1 excess of OVA to YOVA gave a similar spectrum to that at a 3 : 1 excess of OVA to YOVA, where peaks for Ag_1Ab_1 complex were still observed with significant intensities (not shown).

The mass spectrum of O1-1 anti-OVA mAb was similar to that for YOVA (not shown). The mass spectra recorded for a solution of OVA and O1-1, are shown in Fig. 2 D–F. Similarly, an additional two series of peaks for Ag_1Ab_1 and Ag_2Ab_1 complexes with their average charges of +26 and +29, respectively, are seen. Interestingly, peaks for unbound O1-1 are still observed at a 6 : 1 excess of OVA to O1-1, although the MS condition for OVA and O1-1 solution is same as that for OVA and YOVA solution. These results suggest a lower affinity of O1-1 for OVA than that of YOVA. Also, peaks of complex formed between four molecules of OVA and O1-1 dimer (Ag_4Ab_2 complex) was also observed with low intensities as shown in Fig. 2F.

Interaction between immobilized Ags and free mAbs observed by SPR

When the binding of free mAbs to immobilized Ags on a CM5 sensor chip was analyzed (Fig. 3), the binding stoichiometry could not be determined using this procedure because of the difficulty of estimating the number of epitopes on the chip available for the interaction. Therefore the apparent K_a values were estimated from the Scatchard plot or from the ratio of apparent rate constants. As shown in Fig. 3E, Scatchard plots for the binding of O1-1 to immobilized OVA were curved. This can be explained by the formation of two types of complex; a divalent complex formed from two Fab arms at lower mAb concentrations and a monovalent complex using one Fab arm, which appeared at higher mAb concentrations. At a lower mAb concentration, the slope provided K_a value of 2.9×10^7 M^{-1}, which was 85-fold higher than that obtained from sedimentation equilibrium measurements.

Binding of the other mAbs did not attain equilibrium and could not be analyzed using Scatchard plots, especially at lower mAb concentrations (Fig. 3A,B,D). We therefore analyzed association and dissociation kinetics according the procedure recommended by Biacore (Table 2). The validity of this method was confirmed by analyzing O1-1, which had a K_a value obtained using the kinetic method and that was in good agreement with that obtained from Scatchard analysis at low mAb concentrations. The $k_{on,\ app}$, $k_{off,\ app}$, and $K_{a,\ app}$ values in Table 2 indicated that both monoclonal anti-OVA and anti-BSA mAbs were able to bind to the immobilized Ags with a higher K_a value than to free Ags, as determined using AUC, indicating that these mAbs bound bivalently to OVA or BSA immobilized on the sensor chip. It is well known that a bivalent Ag–Ab interaction strengthens the association and provides higher apparent K_a value.

Interaction between free Ags and immobilized mAbs observed by SPR

Binding of Ags, HEL, OVA, and BSA, was analyzed using sensor chips on which the respective mAbs had been immobilized through RAMFc. Typical sensorgrams for the binding of the Ag to the immobilized mAbs on the CM5 chip are shown in Fig. 4A–E. In the case of OVA and O1-1, the interaction was

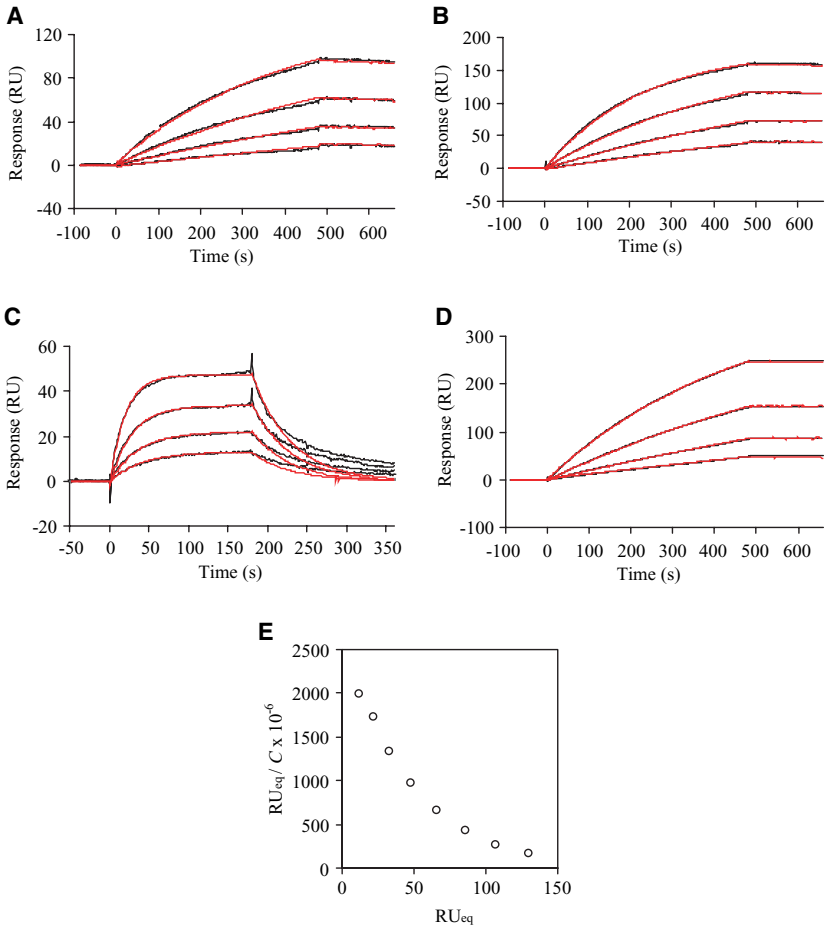


Fig. 3. SPR analysis of interactions between immobilized Ags and free mAbs. (A–D) Sensorgrams for the interaction between HEL and HC1 anti-HEL (0.39–3.1 nM) or HEL and HC2 anti-HEL mAb (0.39–3.1 nM) (A and B), between OVA and O1-1 anti-OVA mAb (6.25–50 nM) (C), and between BSA and KM10 anti-BSA mAb (0.39–3.1 nM) (D) are shown. The sensorgrams (solid black lines) were subjected to nonlinear fitting (dotted red line) to estimate the $k_{on,\ app}$ and $k_{off,\ app}$ values, respectively. (E) Scatchard plots for O1-1 anti-OVA mAb binding to immobilized OVA at a concentration of 6.25–800 nM.

Table 2. Kinetic parameters for interactions between mAbs and immobilized Ags on the sensor chip, CM5.

mAb	$k_{on,\ app}$ ($M^{-1}\cdot s^{-1}$)	$k_{off,\ app}$ (s^{-1})	$K_{a,\ app}$ (M^{-1}) [a]	$K_{a,\ Sca}$ (M^{-1}) [b]
HC1	7.8×10^5	1.2×10^{-4}	6.5×10^9	
HC2	1.4×10^6	5.8×10^{-5}	2.3×10^{10}	
O1-1	6.5×10^5	2.1×10^{-2}	3.1×10^7	2.9×10^7
KM10	6.8×10^5	1.2×10^{-5}	5.6×10^{10}	

[a] $K_{a,\ app}$ was calculated from the two kinetic rate constants, $K_{a,\ app} = k_{on,\ app}/k_{off,\ app}$. [b] $K_{a,\ Sca}$ was determined using Scatchard analysis.

evaluated using Scatchard plot analysis (Fig. 4F), because the reaction proceeded rapidly and attained equilibrium within the measurement time. The plot was linear with a K_a value of 2.4×10^5 M^{-1}, which coincided with that obtained using AUC. However, the RU_{max} value obtained from the abscissa intercept was 0.9, indicating that Ag_1Ab_1 was formed, even in the presence of a large excess of OVA.

Because of the high affinity, RU_{max} values were obtained directly from the sensorgrams in the case of mAbs HC1, HC2, YOVA, and KM10, within an Ag concentration of 400–12 800 nM. Binding stoichiometries for the respective Ag–mAb interactions, together with the kinetic parameters for binding are summarized in Table 3. The results clearly show that a an anti-HEL mAb can bind two HEL molecules simultaneously, whereas anti-OVA or anti-BSA mAbs can bind only a single molecule of OVA or BSA, respectively.

The size-dependent behavior of protein Ags suggested that proteins larger than HEL, such as OVA or BSA, prevented the simultaneous binding of two molecules to the combining sites. This was obviously caused by immobilization of mAbs to the sensor chip and might have been due to the environment in which the mAbs were immobilized. Therefore, we performed SPR measurements using other types of chip such as CM4 and C1. The standard chip, CM5, has a matrix of carboxymethylated dextran covalently attached to a gold surface, as does CM4, but with a lower degree of carboxymethylation, whereas C1 is matrix free and carboxymethylated directly to the gold surface, which

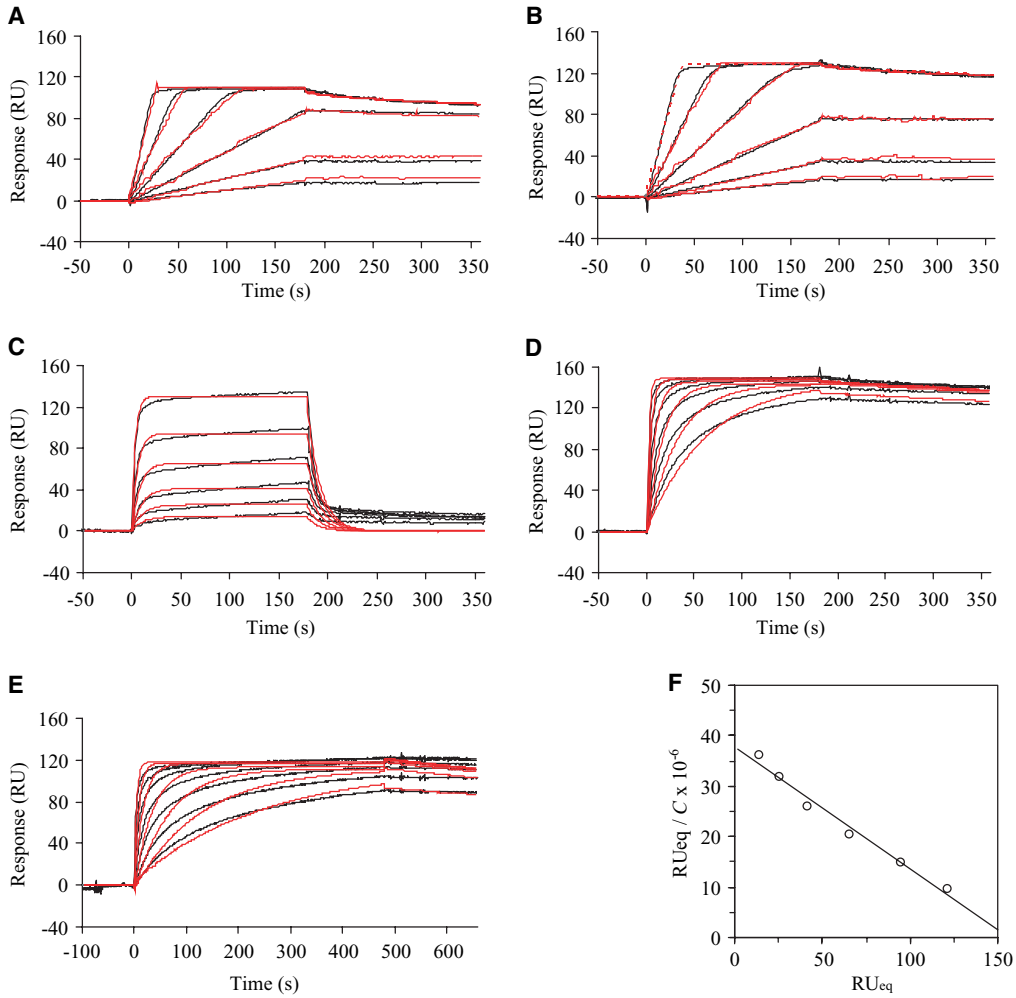


Fig. 4. SPR analysis of interactions between Ags and immobilized mAbs. (A–E) Sensorgrams for the interactions between HEL and HC1 anti-HEL mAb (A), between HEL and HC2 anti-HEL mAb (B), between OVA and O1-1 anti-OVA mAb (C), between OVA and YOVA anti-OVA mAb (D), and between BSA and KM10 anti-BSA mAb (E). Measurements were made at a concentration range of 0.78–25 nM for HEL, 400–12 800 nM for OVA, and 25–1600 nM for BSA. Sensorgrams (solid black lines) were subjected to nonlinier fitting (dotted red line) to estimate the k_{on} and k_{off} values. The amounts of mAb immobilized by RAMFc Ab on the CM5 sensor chip were 650 RU of HC1, 650 RU of HC2, 608 RU of O1-1, 490 RU of YOVA, and 243 RU of KM10, respectively. (F) Scatchard plots for OVA binding to immobilized O1-1 anti-OVA mAb at a concentration of 400–12 800 nM.

Table 3. Binding stoichiometry and kinetic parameters for interactions between Ags and immobilized mAbs on the sensor chip, CM5.

mAb	n [a]	k_{on} ($M^{-1}\cdot s^{-1}$)	k_{off} (s^{-1})	$K_{a,\ kin}$ (M^{-1}) [b]	$K_{a,\ Sca}$ (M^{-1}) [c]
HC1	1.8	1.0×10^8	3.1×10^{-3}	3.2×10^{10}	
HC2	2.1	1.5×10^8	2.7×10^{-3}	5.5×10^{10}	
O1-1	0.9	1.6×10^4	7.7×10^{-2}	2.1×10^5	2.4×10^5
YOVA	1.0	3.9×10^4	3.5×10^{-4}	1.1×10^8	
KM10	1.1	1.5×10^5	4.5×10^{-4}	3.3×10^8	

[a] Binding stoichiometry of Ag to mAb. [b] $K_{a,\ kin}$ was calculated from the two kinetic rate constants, $K_{a,\ kin} = k_{on}/k_{off}$. [c] $K_{a,\ Sca}$ was determined by Scatchard analysis.

is especially beneficial for analyzing interactions with large molecules. As shown in Table 4, the binding stoichiometries were similar to those obtained using the CM5 sensor chip, indicating that the difference in the chip environment had little effect on Ag–Ab interactions in terms of stoichiometry.

Discussion

In this study, we used the soluble proteins HEL, OVA, and BSA as Ags. Based on the crystal structures of HEL, OVA, and human serum albumin, their maximum diameters were calculated to be ~50, 75, and

Table 4. Binding stoichiometry for interactions between Ags and immobilized mAbs on the sensor chips, CM4 and C1.

mAb	CM4 RU_{Ab}	RU_{max} [a]	n [b]	C1 RU_{Ab}	RU_{max} [a]	n [b]
HC1	680	103	1.6	243	44	1.9
HC2	555	103	1.9	262	50	2.0
O1-1	590	180	1.0	305	83	0.9
YOVA	508	156	1.0	310	105	1.1
KM10	332	183	1.2	245	130	1.2

[a] RU_{max} was obtained directly from the sensorgrams for the binding of HC1, HC2, YOVA, and KM10, and was determined by Scatchard analysis for O1-1. [b] Binding stoichiometry of Ag to mAb.

90 Å, respectively [17–19]. By analyzing the stoichiometries of Ag–mAb interactions, we attempted to estimate the capability of mAbs to accommodate Ags of different size, which was expected to be related to the molecular flexibility of the respective mAbs.

Ag–Ab interactions with monovalent Ags can be described by model A in Fig. 5, in which two intermediates, A-II and A-III, are assumed to form, because IgG possesses two combining sites per molecule. However, it is well established that the two combining sites are identical (equivalent), with a special exception, for example, asymmetric Ab as a result of steric hindrance due to the presence in one of the combining sites of a oligosaccharide attached to the Fv region [20], and that the binding of Ags proceeds independently in the case of small Ags such as haptens. Therefore, the model can be simplified to model B in Fig. 5, in which two intermediates are not discriminated between and a single intermediate, B-II is assumed to form, which then converts to the final product, B-III. However, it is not certain whether model B holds true in the case of protein Ags with a high molecular mass. The results of sedimentation equilibrium analysis provided evidence that the binding stoichiometry of Ag to anti-OVA mAb (O1-1) and to anti-BSA mAb (KM10) was 2 in the presence of excess Ags, indicating that model B would apply to Ags such as OVA and BSA. Furthermore, sedimentation equilibrium profiles in the presence of excess Ags to mAbs were described by a single K_a value for both OVA and BSA. This indicates that the two combining sites are equivalent and independent of each other in solution. This conclusion is supported by the results obtained from MS. Observation of Ag_1Ab_1 complex, as well as Ag_2Ab_1 complex, in MS at a low excess of OVA over mAbs indicates the high resolution of this technique.

Because of the molecular mass of HEL, two HEL molecules were expected to bind to anti-HEL mAb. In fact, the interaction between HEL and immobilized anti-HEL mAb detected with SPR showed that two

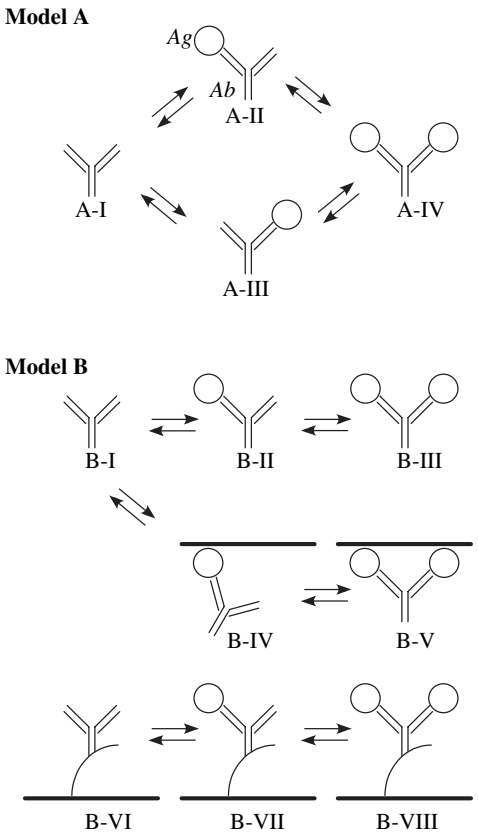


Fig. 5. Models for the binding of Ags to the respective mAbs. In general, Ag–Ab interactions can be described by model A. When Abs and Ags are free in solution, Ab (A-I) can bind two Ag molecules via intermediates (A-II and A-III) and form an Ag_2Ab_1 complex (A-IV). Because the two combining sites are equivalent and independent of each other, the interaction can be described by a more simple form such as model B, assuming a single intermediate (B-II) that is able to convert to Ag_2Ab_1 complex (B-III). The apparent association constants for the first process (K_1) and for the second process (K_2) are related as follows: $K_1 = 4K_2$. When Ags are immobilized, Ab (B-I) can form a bivalent complex (B-V) via an intermediate (B-IV). Because SPR cannot distinguish B-IV from B-V, the observed association constant (K_{app}) is defined as $K_{app} = K_1 \times K_2$. When Ab is immobilized on the sensor chip by RAMFc (B-VI), the first Ag molecule can bind to one of the combining sites with K_1. In the case of OVA or BSA, however, the second Ag molecule cannot bind due to steric hindrance of the first bound Ag. Such hindrance is not observed in the interaction between HEL and anti-HEL mAbs.

HEL molecules bound to a anti-HEL mAb simultaneously, as described below. Based on the results of the cryo-ET experiments in which one Fab arm of IgG2a could open to a maximal 141° relative to the other Fab arm [5,6], the distance between the two combining sites was calculated to be ~130 Å. When the three components, two Fab arms and one Fc region, can move freely in solution, an Ab molecule

has the ability to bind to two protein Ags simultaneously. Therefore, Ab molecules possess sufficient flexibility to accommodate protein Ags with a size of 50–90 Å. This simultaneous binding with two Fab arms was also observed in the interaction between free mAbs and Ags immobilized on the sensor chips (Fig. 3 and Table 2). The Abs were able to cross-link two Ag molecules on the chip (B-V in Fig. 5) and acquire high avidity via this bivalent interaction.

The SPR measurements for the interaction between OVA or BSA and the respective mAbs immobilized on the chip through RAMFc showed that the Ags bound to the mAbs at a ratio of 1 : 1 (B-VII). Because the binding of HEL showed an Ag/mAb ratio of 2 : 1 (B-VIII), there was a clear difference between HEL and OVA or BSA. This difference did not depend on the magnitude of K_a (Table 2). Therefore, Abs immobilized to the chip via the Fc region were able to form the intermediate B-VII with all protein Ags, but were not capable of providing the final product, B-VIII, in the case of OVA or BSA. Because two Ag molecules can bind to a mAb molecule when they are free in solution, it seems likely that the incomplete binding of OVA or BSA seen in SPR measurements arises from decreased movement of the Fab arms by immobilization of mAbs.

Although the stoichiometry was altered by immobilization of anti-OVA and anti-BSA mAbs, the K_a values obtained by AUC and SPR were in accord with each other. This showed that the binding of the first Ag molecule proceeded without hindrance in SPR experiments, suggesting that the reduction in stoichiometry was not caused by bulk effects from the sensor chip. Although we initially considered that the neighboring mAbs might inhibit the binding of large protein Ags, this is less likely because the SPR measurements were carried out under conditions in which the RU_{Ab} value was $\sim$300 RU, which corresponded to a single mAb molecule in an area of 83 000 Å^2. In addition, substituting the CM5 chip with a CM4 or C1 provided little change in the stoichiometry. Therefore, we concluded that the inability to form the trimolecular complex, Ag_2Ab_1, was not due to steric hindrance by neighboring mAbs or to a bulk effect from the chip but rather to interference by the Ag which bound first. This means that immobilization through the Fc regions would result in restriction of movement and reduction of the segmental flexibility of the Fab arms, which would allow only HEL to form of an Ag_2Ab_1 complex and not OVA or BSA. Previously, we showed that Ag binding to the combining sites in Fv domains induced conformational changes around the binding sites for staphylococcal protein A in the C_H2–C_H3 domain [15,16]. Therefore, it is likely that not only two Fab arms but also the Fc region would contribute to the Ag binding. If the Fc region does not move freely, the Fab arms cannot be fully functional. Because Abs bound to FcR as well as BCR are immobilized through the Fc regions, it is possible that the dynamic range of their Fab arms is restricted under these conditions, causing them to behave differently in interactions with Ags compared with Abs free in solution. A future study will clarify the relationship between segmental flexibility and the Ag binding of BCRs.

In this study, AUC, MS, and SPR were used to characterize protein–protein interactions. Sedimentation equilibrium analysis, which is one of two representative methods of AUC, provides molecular mass information and is based on the sedimentation properties. In the case of sedimentation equilibrium analysis, the total concentration gradient profile in solution at equilibrium is acquired, from which we can readily estimate information on averaged molecular mass. Stoichiometry and equilibrium constant between interacting molecules are also obtained by nonlinear least-squares fitting of the concentration gradient, although the fitting analysis is dependent upon the choice of model and the complexes present in solution have to be assumed for the analysis. Meanwhile, MS using a gentle desolvation technique and controlled pressure conditions is able to provide a direct and precise measure of the molecular mass of noncovalently associated protein complexes and hence the stoichiometry of interacting partners. The method is independent of the shape of the complex and provides an estimate of all species present in solution. Although MS is performed in the gas phase use of appropriate conditions ensures that no dissociation of the complexes is occurring. The two approaches are, therefore, entirely complimentary and the good agreement found between the two methodologies provides us with convincing conclusions for our interaction analysis.

Experimental procedures

Ag and mAb preparation

HEL was purchased from Wako Pure Chemical Industries (Osaka, Japan) and OVA and BSA were purchased from Sigma (St. Louis, MO), and all of these were used without further purification. Hybridomas producing anti-HEL IgG1s, HC1 and HC2, and anti-OVA IgG1s, O1-1 and YOVA, were cultured in Iscove's modified Dulbecco's medium containing 10% fetal bovine serum. The mAbs secreted into the medium were purified using an Ag column and were

then dialyzed against NaCl/P_i. KM10, an anti-BSA IgG1, was kindly provided by Kyowa Hakko Kogyo Co., Ltd (Tokyo, Japan). RAMFc was purchased from Biacore. Protein concentrations were determined at an A of 280 nm using molar absorption coefficients of 3.85×10^4 M^{-1}·cm^{-1} for HEL, 3.21×10^4 M^{-1}·cm^{-1} for OVA, 4.60×10^4 M^{-1}·cm^{-1} for BSA, and 2.10×10^6 M^{-1}·cm^{-1} for mAbs.

Analytical ultracentrifugation

All AUC experiments were carried out in NaCl/P_i solution. Sedimentation equilibrium experiments were performed with an XL-A or XL-I analytical ultracentrifuge (Beckman-Coulter Inc., Fullerton, CA) at 20 °C using a double-sector charcoal-filled epon centerpiece (1.2 cm) with sapphire windows. The rotor (An-50Ti, Beckman-Coulter Inc.) speeds used were 2880 ***g***, 5130 ***g*** and 11 530 ***g***. Prior to interaction experiments, apparent molecular masses, M_{app}, of Ags and mAbs at different concentrations covering those used in the interaction experiments were estimated. M_{app} values of Ags and mAbs were obtained by nonlinear least squares fitting of the data using the following Eqn (1),

$$A(r) = A_0(r_0)\exp[H(1-\nu\rho)M_{app}(r^2 - r_0^2)] + B \qquad (1)$$

where

$$H = \frac{(\omega/2\pi)^2}{2RT}$$

ν is the partial specific volume of the sample, ρ is the density of the solvent, R is the gas constant, T is temperature, ω is the rotor speed in r.p.s. units, A_0 is the absorbance at a reference point, r_0, Ar is the absorbance at a position r cm from the rotor center and B is the baseline correction. In this study, the ν of each sample was calculated based on its amino acid composition.

Regarding interaction analyses, concentrations of mAbs were fixed at 1.65 or 3.3 μM, whereas those for Ags were changed from 1.65 to 19.8 μM, which provided molar ratios of Ags to mAbs of 1 : 2, 1 : 1, 3 : 1, and 6 : 1. Data were collected and the average of eight measurements at each radial distance was calculated. Approach to equilibrium was considered to be complete when replicate scans separated by 6 h intervals were indistinguishable. Nonlinear least square fitting using the 1 : 1 (Ag/mAb) binding model (Eqn 2), or the 2 : 1 (Ag/mAb) binding model (Eqn 3), were performed to determine stoichiometry and K_a [21,22],

$$\begin{aligned} A(r) = {} & A_{0,Ag}(r_0)\exp[H(1-\nu_{Ag}\rho)M_{Ag}(r^2 - r_0^2)] \\ & + A_{0,Ab}(r_0)\exp[H(1-\nu_{Ab}\rho)M_{Ab}(r^2 - r_0^2)] \\ & + A_{0,Ag}(r_0)A_{0,Ab}(r_0)\exp[(H(1-\nu_{Ag}\rho)M_{Ag} \\ & + H(1-\nu_{Ab}\rho)M_{Ab})(r^2 - r_0^2) + \ln[k]] + B \end{aligned} \qquad (2)$$

$$\begin{aligned} A(r) = {} & A_{0,Ag}(r_0)\exp[H(1-\nu_{Ag}\rho)M_{Ag}(r^2 - r_0^2)] \\ & + A_{0,Ab}(r_0)\exp[H(1-\nu_{Ab}\rho)M_{Ab}(r^2 - r_0^2)] \\ & + [A_{0,Ag}(r_0)]^2 A_{0,Ab}(r_0)\exp[(H(1-\nu_{Ag}\rho)2M_{Ag} \\ & + H(1-\nu_{Ab}\rho)M_{Ab})(r^2 - r_0^2) + \ln[k]] + B \end{aligned} \qquad (3)$$

M_{Ag} and M_{Ab} represent the molecular masses of each Ag and mAb, respectively, and were obtained from Ag and mAb measurements. Each k-value was converted to K_a based on Eqn (4) for the 1 : 1 model or Eqn (5) for the 2 : 1 model using the extinction coefficients of each component.

$$K_a = \frac{k\varepsilon_{Ab}\varepsilon_{Ag}l}{\varepsilon_{Ab} + \varepsilon_{Ag}} \qquad (4)$$

$$K_a^2 = \frac{k\varepsilon_{Ab}\varepsilon_{Ag}l^2}{\varepsilon_{Ab} + 2\varepsilon_{Ag}} \qquad (5)$$

$\varepsilon_{Ab} + 2\varepsilon_{Ag}$ where ε_{Ab} and ε_{Ag} are molar absorption coefficients of mAb and Ag, respectively, and l is the path length of the centerpiece. All nonlinear least squares fittings were performed using MATHEMATICA 5.1 (Wolfram Research Inc., Champaign, IL) employing the Levenberg–Marquart algorithm.

Mass spectrometry

Concentrations of anti-OVA mAbs were fixed to 16 μM for YOVA and 7 μM for O1-1, whereas those for Ag, OVA, were changed to give different Ag/mAb molar ratios of 1 : 1, 3 : 1, and 6 : 1. Sample solutions of Ag, mAbs, and their complexes were prepared in NaCl/P_i, followed by buffer exchange to 150 mM ammonium acetate, pH 7.5, through Bio-Spin 6 column before analysis.

All samples were analyzed by nanoflow electrospray using capillaries prepared as described previously [23]. Two-microliter aliquots of sample were loaded into capillaries, and spectra were recorded on a modified Micromass QTOF2 mass spectrometer (Waters, Manchester, UK). This modified mass spectrometer consists of a nanoflow electrospray interface, a low-frequency extended mass range quadrupole, followed by a hexapole collision cell and a TOF mass analyzer [24]. The capillary and cone voltage were maintained at 1800 and 120 V, respectively. Pressure conditions were maintained at 4×10^{-3} mbar in the hexapole ion guide. All mass spectra were calibrated against cesium iodide and analyzed using MASS LYNX software (Waters).

SPR measurement

The Biacore biosensor system, Biacore 2000 (Biacore AB, Uppsala, Sweden), was used to measure real-time Ag–mAb interactions. Two types of measurements were made by immobilizing either the Ags or mAbs. While protein Ags were covalently linked to a CM5 sensor chip for their

immobilization, mAbs were captured through RAMFc covalently linked to sensor chips, CM5, CM4, and C1, as described previously [12]. In the latter case, becaue of the different degree of carboxymethylation on the respective sensor chip surfaces, the amounts of RAMFc covalently coupled to the chips differed as follows: ~1500 RU for C1, 4500 RU for CM4, and 8000 RU for CM5. A solution of mAbs (12.5–400 nM) in NaCl/P_i containing 0.005% Tween 20 was then applied to the RAMFc chip at a rate of 20 μL·min^{-1} over a course of 30 s, which resulted in the capture of 200–1000 RU. In order to evaluate Ag–mAb interactions, mAbs or Ags were diluted to various concentrations in NaCl/P_i containing 0.005% Tween 20 and applied over sensor chips coupled with immobilized Ags or mAbs, at a rate of 20 μL·min^{-1} for 3 or 8 min. The Ag and RAMFc chips were regenerated with one and three 15 μL injections of 10 mM glycine buffer (pH 1.8), respectively. All experiments were performed at 25 °C.

The sensorgrams for Ag–mAb interactions were then examined by first adjusting for background changes reflected by the bulk refractive indices which were obtained from sensorgrams of interactions between Ags and negative control mAbs immobilized on the RAMFc chips, or between mAbs and the negative control protein Ags. The binding stoichiometry (n) was determined using Eqn (6), assuming the molecular mass of the mAb to be 150 kDa.

$$n(\mathrm{Ag/mAb}) = \frac{\mathrm{RU_{max}}}{\mathrm{RU_{Ab}}} \times \frac{1.5 \times 10^5}{\mathrm{MW_{Ag}}} \quad (6)$$

where RU_{max} is the total surface binding capacity, RU_{Ab} is the amount of mAb immobilized through RAMFc on the sensor chip, and MW_{Ag} is the molecular mass of the Ag. RU_{max} could be determined by the sensorgrams directly, or by Scatchard analysis using Eqn (7).

$$\mathrm{RU_{eq}}/C = K_a \times \mathrm{RU_{max}} - K_a \times \mathrm{RU_{eq}} \quad (7)$$

where C is the free analyte concentration, K_a is the association constant, and RU_{max} is the steady-state response. Kinetic data were analyzed using BIAEVALUATION 3.2 software, which was supplied with the Biacore system. In this program, a global fitting method was used to determine the association and dissociation rate constants, k_{on} and k_{off}, using a model of 1 : 1 Langmuir binding to an immobilized mAb.

$$K_{a,\,kin} = k_{on}/k_{off} \quad (8)$$

In the case of immobilized Ags, the apparent rate constants for association ($k_{on,\,app}$) and dissociation ($k_{off,\,app}$) were estimated. The apparent K_a value ($K_{a,\,app}$) was defined by Eqn (9).

$$K_{a,\,app} = k_{on,\,app}/k_{off,\,app} \quad (9)$$

Acknowledgements

The authors thank Dr Akemi Ota and Ms Maiko Yoshida for preparing mAbs and Dr Damien Hall for helpful comments for the manuscript. The authors also thank Dr William Campbell for English editing of the manuscript. The anti-BSA mAb, KM10, was kindly provided by Kyowa Hakko Kogyo Co., Ltd. This study was partly supported by grants from the Japanese Ministry of Education, Science and Culture to MO and SU.

References

1 Jefferis R, Lund J & Pound JD (1998) IgG-Fc-mediated effector functions: molecular definition of interaction sites for effector ligands and the role of glycosylation. *Immunol Rev* **163**, 59–76.
2 Harris LJ, Larson SB, Hasel KW & McPherson A (1997) Refined structure of an intact IgG2a monoclonal antibody. *Biochemistry* **36**, 1581–1597.
3 Harris LJ, Skaletsky E & McPherson A (1998) Crystallographic structure of an intact IgG1 monoclonal antibody. *J Mol Biol* **275**, 861–872.
4 Roux KH, Strelets L & Michaelsen TE (1997) Flexibility of human IgG subclasses. *J Immunol* **159**, 3372–3382.
5 Bongini L, Fanelli D, Piazza F, De Los Rios P, Sandin S & Skoglund U (2004) Freezing immunoglobulins to see them move. *Proc Natl Acad Sci USA* **101**, 6466–6471.
6 Sandin S, Ofverstedt LG, Wikstrom AC, Wrange O & Skoglund U (2004) Structure and flexibility of individual immunoglobulin G molecules in solution. *Structure* **12**, 409–415.
7 Kato K, Sautes-Fridman C, Yamada W, Kobayashi K, Uchiyama S, Kim H, Enokizono J, Galinha A, Kobayashi Y, Fridman W-H *et al.* (2000) Structural basis of the interaction between IgG and Fcγ receptors. *J Mol Biol* **295**, 213–224.
8 Aquilina JA, Benesch JL, Bateman OA, Slingsby C & Robinson CV (2003) Polydispersity of a mammalian chaperone: mass spectrometry reveals the population of oligomers in αB-crystallin. *Proc Natl Acad Sci USA* **100**, 10611–10616.
9 Ilag LL, Ubarretxena-Belandia I, Tate CG & Robinson CV (2004) Drug binding revealed by tandem mass spectrometry of a protein–micelle complex. *J Am Chem Soc* **126**, 14362–14363.
10 Ilag LL, Videler H, McKay AR, Sobott F, Fucini P, Nierhaus KH & Robinson CV (2005) Heptameric (L12), 6/L10 rather than canonical pentameric complexes are found by tandem MS of intact ribosomes from thermophilic bacteria. *Proc Natl Acad Sci USA* **102**, 8192–8197.

11 Tito MA, Miller J, Walker N, Griffin KF, Williamson ED, Despeyroux-Hill D, Titball RW & Robinson CV (2001) Probing molecular interactions in intact antibody: antigen complexes, an electrospray time-of-flight mass spectrometry approach. *Biophys J* **81**, 3503–3509.
12 Oda M & Azuma T (2000) Reevaluation of stoichiometry and affinity/avidity in interactions between antihapten antibodies and mono- or multi-valent antigens. *Mol Immunol* **37**, 1111–1122.
13 Oda M, Sato-Nakamura N & Azuma T (2004) Molecular characterization of monovalent and multivalent hapten–protein conjugates for analysis of the antigen–antibody interaction. *Anal Biochem* **333**, 365–371.
14 Tobita T, Oda M & Azuma T (2004) Segmental flexibility and avidity of IgM in the interaction of polyvalent antigens. *Mol Immunol* **40**, 803–811.
15 Oda M, Kozono H, Morii H & Azuma T (2003) Evidence of allosteric conformational changes in the antibody constant region upon antigen binding. *Int Immunol* **15**, 417–426.
16 Sagawa T, Oda M, Morii H, Takizawa H, Kozono H & Azuma T (2005) Conformational changes in the antibody constant domains upon hapten-binding. *Mol Immunol* **42**, 9–18.
17 Motoshima H, Mine S, Masumoto K, Abe Y, Iwashita H, Hashimoto Y, Chijiiwa Y, Ueda T & Imoto T (1997) Analysis of the stabilization of hen lysozyme by helix macrodipole and charged side chain interaction. *J Biochem* **121**, 1076–1081.
18 Stein PE, Leslie AG, Finch JT & Carrell RW (1991) Crystal structure of uncleaved ovalbumin at 1.95 Å resolution. *J Mol Biol* **221**, 941–959.
19 Bhattacharya AA, Curry S & Franks NP (2000) Binding of the general anesthetics propofol and halothane to human serum albumin. High resolution crystal structures. *J Biol Chem* **275**, 38731–38738.
20 Margni RA & Maran Borel I (1998) Paradoxical behavior of asymmetric IgG antibodies. *Immunol Rev* **163**, 77–87.
21 Lewis MS, Shrager RI & Kim SJ (1994) Sedimentation equilibrium. In *Modern Analytical Ultracentrifugation* (Shuster TM & Laue TM, eds), pp. 94–118. Birkhaeuser, Boston.
22 Lebowitz J, Lewis MS & Schuck P (2002) Modern analytical ultracentrifugation in protein science: a tutorial review. *Protein Sci* **11**, 2067–2079.
23 Nettleton EJ, Sunde M, Lai Z, Kelly JW, Dobson CM & Robinson CV (1998) Protein subunit interactions and structural integrity of amyloidogenic transthyretins: evidence from electrospray mass spectrometry. *J Mol Biol* **281**, 553–564.
24 Sobott F, Hernandez H, McCammon MG, Tito MA & Robinson CV (2002) A tandem mass spectrometer for improved transmission and analysis of large macromolecular assemblies. *Anal Chem* **74**, 1402–1407.